Modelling the vibration response of disk-type windings in power transformers

Lingzhi Li (1), Ming Jin (1), Xuhao Du (2), Hai Huang (1) and Jie Pan (2)

(1) Department of Instrument Science and Engineering, Zhejiang University, Hangzhou, 310027, China
(2) Department of Mechanical Engineering, The University of Western Australia, Perth, WA 6009, Australia

ABSTRACT

Winding vibration is one of the most important noise sources in loaded power transformers. However, accurate and effective modelling of the winding vibration response is often hindered by the complicated conductor and insulation material distributions in the winding structure. In this paper, the winding is described by a coupled-ring model, which are applied on three experimental winding structures. The vibration response of the winding to a point force excitation is then analysed using the finite element method. This simplified model allows efficient prediction and understanding of the vibration characteristics of complex winding structures.

1 INTRODUCTION

Power transformers are vital and expensive facilities in the power grid, whose failure may cause enormous losses (Li *et al*., 2017). About one–fifth of faults in transformers happen in the windings (Jin & Pan, 2015). Furthermore, vibrations of windings are one of the most important sources of transformer noise (Rausch *et al*., 2002). In this case, the vibration characteristics of windings are of vital significance for the fault diagnosis and noise control of power transformers. As a common type of winding, the vibration features of disk-type windings have been explained by several models. The natural frequencies of the winding based on a three-element viscoelastic model were presented by Patel (1973), which was one-dimensional and lacking in the information of the radial direction. Booth and McDonald (1998) used an artificial neural network to estimate the winding vibration. However, they did not present clear information on the vibration frequency response functions (FRFs) and resonance frequencies of the windings. It is clear that, in order to have sufficient physical information, more vibration characteristics based on a simplified but efficient model are urgently required.

In this paper, a simplified physical model is used to model the vibration characteristics of disk-type windings. The disk-type winding is described by metal rings coupled by rubbers. Based on this model, the vibration frequency responses of three different coupled rings are measured experimentally and simulated using the finite element method (FEM). Their results are discussed and compared, and some meaningful conclusions are obtained. They may be useful in the noise control and fault diagnosis of power transformers.

2 SIMPLIFIED MODEL FOR DISK-TYPE WINDINGS AND INVESTIGATED RINGS

2.1 The model

The layout of a typical disk-type winding of a power transformer is shown in Figure 1(a). The coil in each layer of the winding is wound in the radial direction, and disk layers are stacked in the axial direction. Conductors inside coils are wrapped with insulation papers for insulation. In order to improve the cooling efficiency, adjacent layers are separated by insulation pressboards.

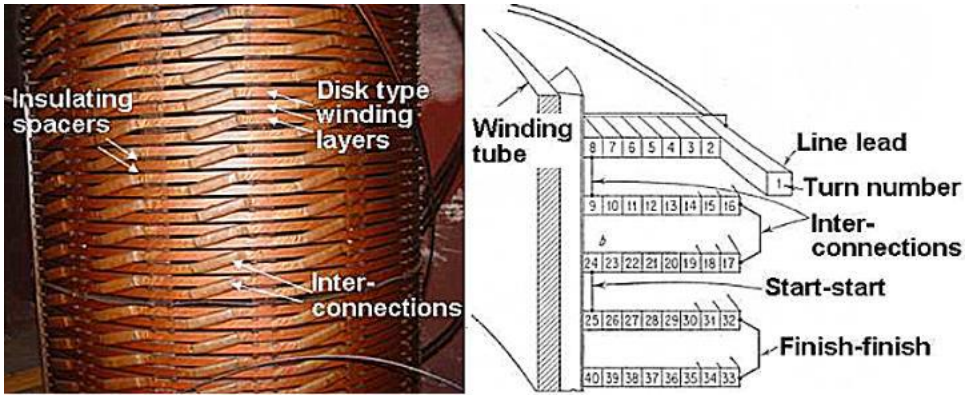

(a)

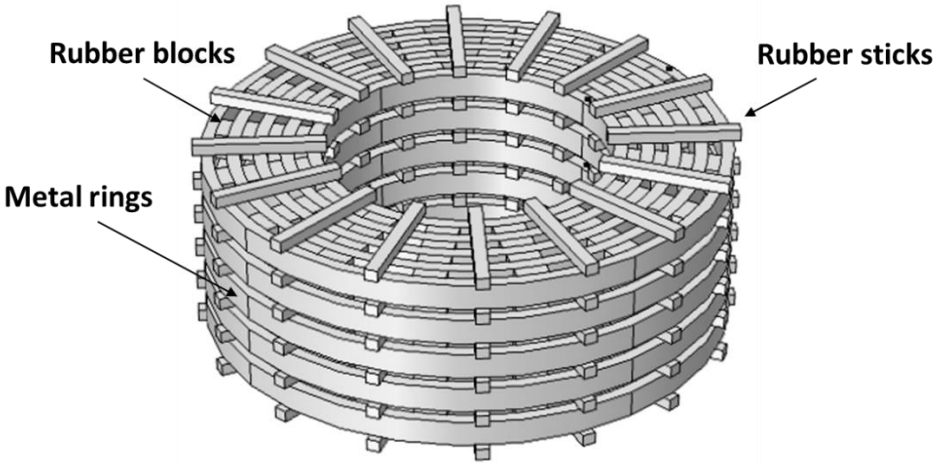

(b)

Figure 1: (a) Typical layout of a disk-type winding in a power transformer and the simplified model rig used in this paper (Nguyen, 2007, Jin, 2015). (b) The simplified model for disk-type windings.

In term of the structure of a disk-type winding, a coupled-ring model (Jin, 2015) is used to describe the vibration response of the winding shown in Figure 1(b). Conductors inside coils are modelled as concentric metal rings. Each ring coupled radially in one layer represents the corresponding coil in a disk layer of the winding, while each layer stacked axially models the corresponding disk. Rubber sticks and blocks are evenly distributed and characterise insulation pressboards between layers and insulation papers wrapping the conductors, respectively. As a nonlinear material, rubber can express the nonlinear stress–strain relationship of insulation papers and pressboards as they absorb and release transformer oil. Although discrete in this model, the rubber blocks represent similar structural features as a rubber circle and are more convenient for research (Jin, 2015).

Equivalent to a disk-type winding, this coupled-ring model can efficiently represent the vibration characteristics of a disk-type winding (Jin, 2015). In addition, being separated from the core of a transformer, this simplified rig makes it possible to conduct research on the winding's vibration response alone. Furthermore, the coupled rings and stacks are easy to adjust, enabling different experimental settings, thus making it easier to analyse different kinds of faults in windings.

2.2 Investigated rings

Figure 2 shows the coupled rings investigated in this paper. Figures 2(a) and (b) show respectively two and five radially coupled rings in a single layer, and Figure 2(c) shows a multi-layer ring stack. Investigation on two and five radially coupled rings is helpful for determining the vibration characteristics in the radial direction and the way that coupled rings vibrate. As the most fundamental stack, the two-by-five coupled-ring stack can help reveal the

structural vibration characteristics in both radial and axial directions, which is a convenient basic model for disk-type windings.

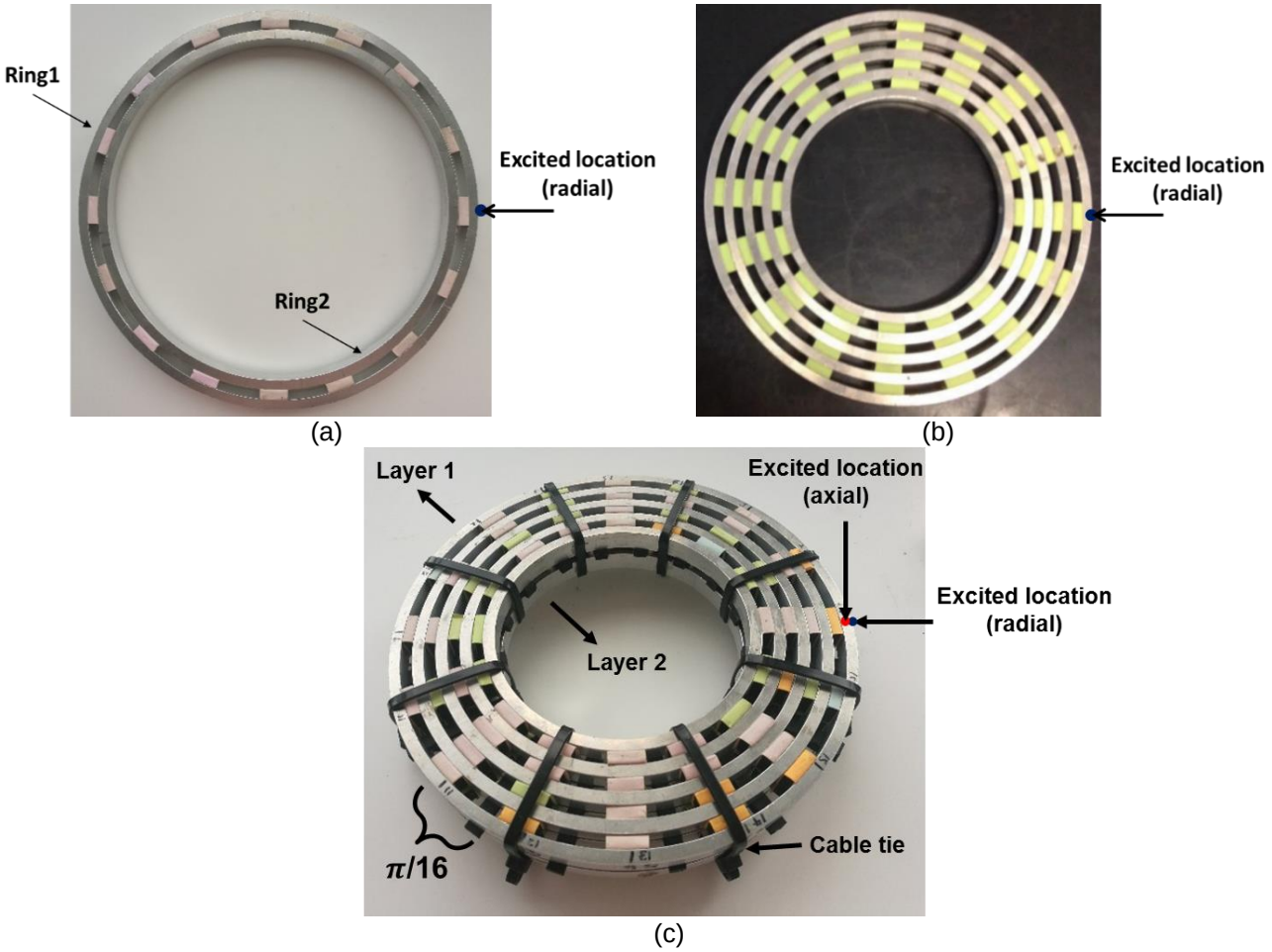

Figure 2: Three different coupled rings investigated in this paper: (a) two radially coupled rings, (b) five radially coupled rings, and (c) a two-by-five coupled-ring stack.

The radiuses (outer radiuses) of coupled rings in one layer decrease from 100 mm with a decrement of 10 mm. Each ring has the same in-plane thickness and width (out-of-plane thickness), which are 5 mm and 10 mm, respectively (*i.e.*, the cross-section area of the rings is $5\ \mathrm{mm}\times 10\ \mathrm{mm}$). The multi-layer ring stack in Figure 2(c) is stacked vertically with two layers of radially coupled rings, as shown in Figure 2(b). Each ring is coupled and stacked carefully to ensure they are concentric. Sixteen rubber blocks and sixteen rubber sticks, which are made from the same material, are evenly inserted between two adjacent rings in one layer and in two adjacent layers in the stack, respectively. For better structural stability, sticks are interlaced with blocks, and thus the in-plane included angle between an adjacent stick and block is $\pi/16$.

Unless otherwise stated, the rings in a layer are named Ring 1 to Ring 5 from the outermost ring to the innermost ring and the layers are named Layer 1 to Layer 2 from the top to the bottom of the stack. The smallest ring in the lower layer of the stack in Figure 2(c), for example, is defined as Ring 5 in Layer 2.

3 EXPERIMENT SETUP

The experimental devices shown in Figure 3 were used to measure the frequency responses of the investigated objects. They were excited by an impact hammer (B&K 8206) and the vibration acceleration was measured by accelerometers (B&K 4274) via charge amplifiers (B&K 2635). The excitation force and the vibration signals were sent to a B&K pulse analyser for computing the FRFs.

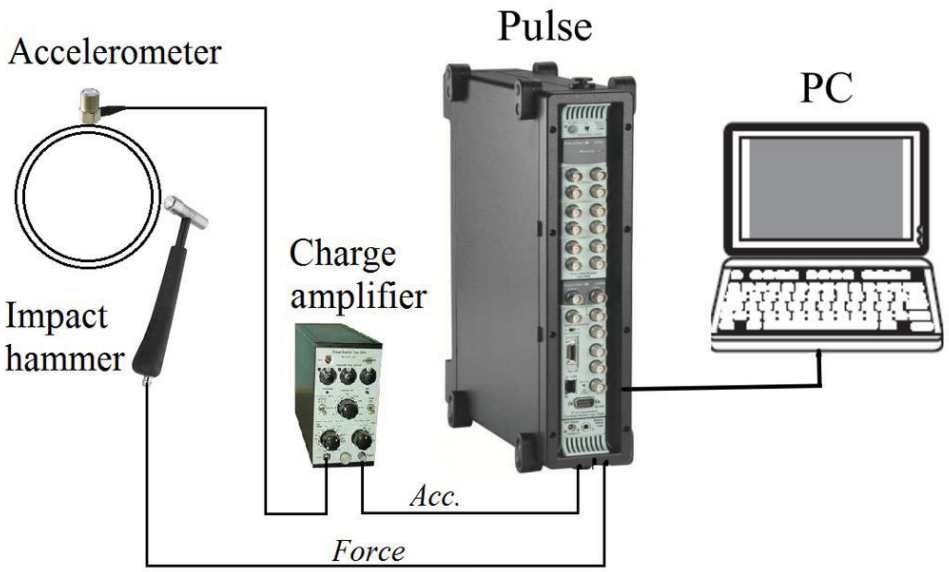

Figure 3: Experiment setup for the measurement of coupled rings' vibration (Jin, 2015).

The plane of the ring containing its centreline is the principal plane of the cross section and also a plane of material symmetry (Chidamparam, 1993). For this model, the rings' in-plane (*i.e.*, radial) and out-of-plane (*i.e.*, axial) vibrations are thus uncoupled. Therefore, the radial and axial vibration responses of the coupled rings were measured separately in this paper, excited in the radial and axial directions, respectively. Both the radial and axial vibrations of the multi-layer ring stack will be analysed, while the single-layer ring is only measured and investigated radially.

The excitation location in the experiment was on Ring 1 of the radially coupled rings, and Layer 1 of the stack, as shown in Figure 2. Each investigated object was hung as a whole by soft cotton threads, so that they were under free boundary conditions on both radial and axial directions. Meanwhile, the two-by-five coupled-ring stack was tied up with eight cable ties. This arrangement imitated the clamping of a disk-type winding and also prevented the movement of ring layers due to hammer tapping. Different locations were measured for each investigated object, details of which can be found in the Results and Discussion section.

4 FEM SIMULATION

The FRFs of the investigated objects were simulated using FEM with COMSOL Multiphysics 5.3a (Structural Mechanics Module, Frequency Analysis Study). The meshes of each simulated objects are shown in Figure 4. The rings used in this research were made of aluminium alloy, and thus were modelled as linear elastic materials in the Solid Mechanics interface. As a hyperelastic material, rubber blocks and sticks were described by a non-linear elastic material model. The accelerometer was not included in the simulation due to its negligible mass compared with whole structure. Referred to the point impulse force of 1 N in the investigated direction, the FRFs on the measurement locations stepped by 10 Hz were calculated based on Eq. 1, where $H(f)$ is FRF, $X(f)$ and $Y(f)$ are excitation force signal and measured vibration signal in frequency domain, respectively. The parameters mainly used in the simulation are listed in Tables 1 and 2.

$$H(f) = 20log_{10}[\frac{Y(f)}{X(f)}] \quad (1)$$

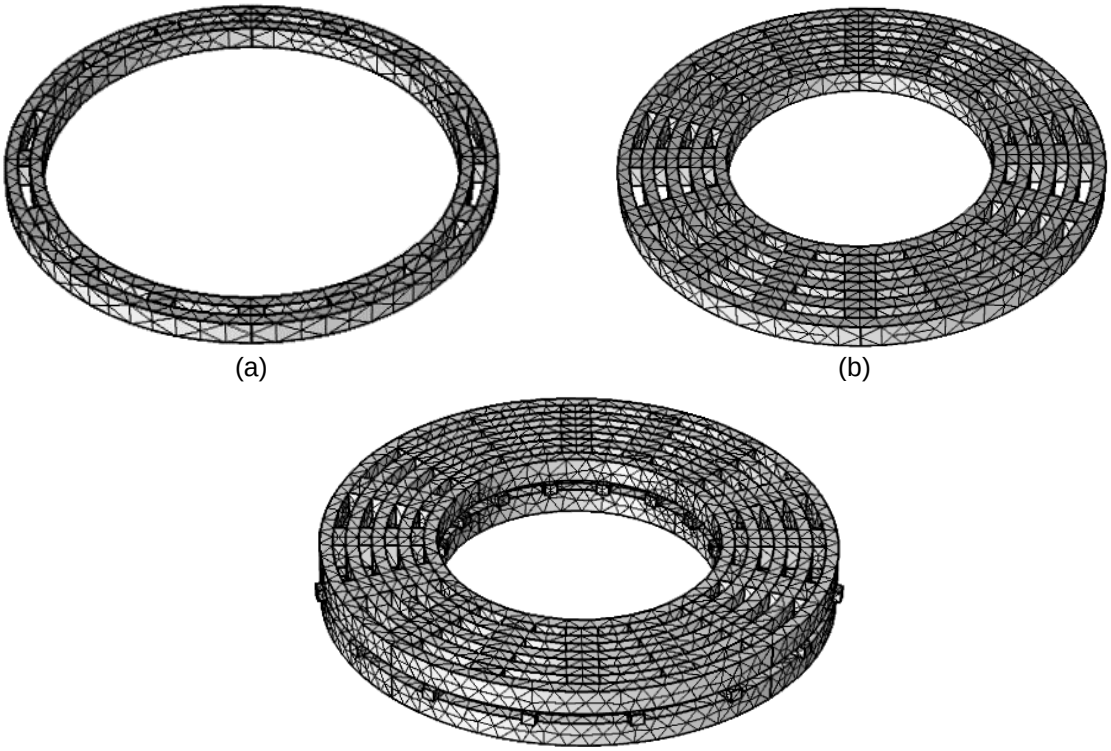

(a) (b)

(c)

Figure 4: Simulation meshes of the investigated objects: (a) two radially coupled rings, (b) five radially coupled rings, and (c) the two-by-five coupled-ring stack.

Table 1: Main parameters of the rings in the simulation.

Parameter	Value
Outer radius, *r* (mm)	100, 90 (two rings in one layer) 100, 90, 80, 70, 60 (five rings in one layer)
In-plane thickness, *t* (mm)	5
Out-of-plane thickness, *h* (mm)	10
Young's modulus, *Ex*, *Ey*, *Ez* (GPa)	70, 70, 70
Shear modulus, *Gx*, *Gy*, *Gz* (GPa)	26, 26, 20
Density, ρ (kg/m^3)	2700
Poisson's ratio, v_x, v_y, v_z	0.33, 0.33, 0.33
Loss factor of Young's modulus, η_x, η_y, η_z	0.02, 0.02, 0.02

Table 2: Main parameters of the rubbers in the simulation.

Parameter	Value
Length, *d* (mm)	12 (block) 50 (stick)
Width, *w* (mm)	10 (block) 5 (stick)
Thickness, *h* (mm)	4.5
Young's modulus, *E* (MPa)	50
Density, ρ (kg/m^3)	1650
Poisson's ratio, *v*	0.49
Loss factor of Young's modulus, η	0.25

5 RESULTS AND DISCUSSION

The experiment and simulation results for each set of coupled rings are presented and discussed in this section. The COMSOL Multiphysics moduli for different coupled rings may be slightly adjusted, owing to divergences in the experiment, within reasonable limits. For two and five radially coupled rings, only radial vibration responses were investigated considering that they were coupled radially. In addition, the ring-stack was measured and simulated in both two directions.

5.1 Two radially coupled rings

Figure 5 shows the mobility FRFs of two radially coupled rings on Ring 1 and Ring 2, included angles of excitation and the measurement locations for 10°, 90°, and 180° in Figure 5(a), (b), and (c), respectively.

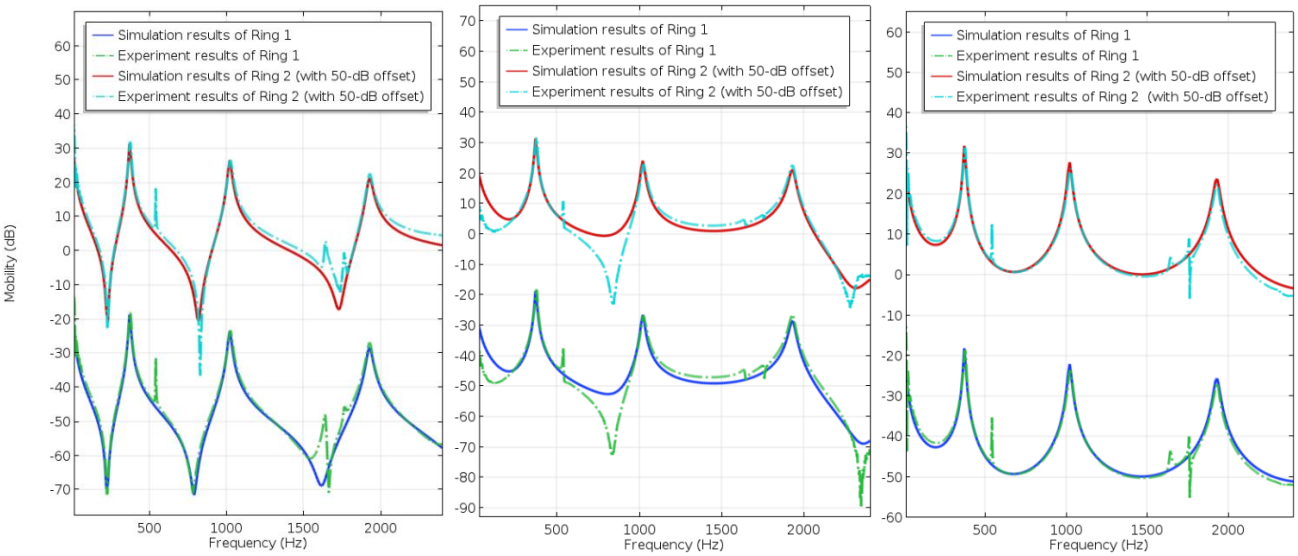

(a) (b) (c)

Figure 5: Comparison of simulation and experiment results for the FRFs of two radially coupled rings in the radial direction at three different included angles of excitation, (a) 10°, (b) 90°, and (c) 180°, on the two rings (for clarity, each curve is offset from the one beneath by 50 dB).

The results from the experiment and simulation agree with each other quite well at all three angles on each ring, which verifies that the FEM simulation settings are reasonable. The small sharp peaks in the FRFs of the experiment results may have been caused by the inevitable experimental errors such as slight deformation of rings due to manufacturing. These results also reveal that the coupled rings vibrate together, as the two rings resonate almost at the same frequencies.

5.2 Five radially coupled rings

Figure 6 shows the FRFs of five radially coupled rings on Ring 1, Ring 3, and Ring 5. As with the two coupled rings, the results of three different locations on three rings are given. It is clear that the simulation results fit well with the experiment ones, though not as good as the two coupled rings. This is reasonable since the difference between the experiment and simulation may grow with the increasing number of rings.

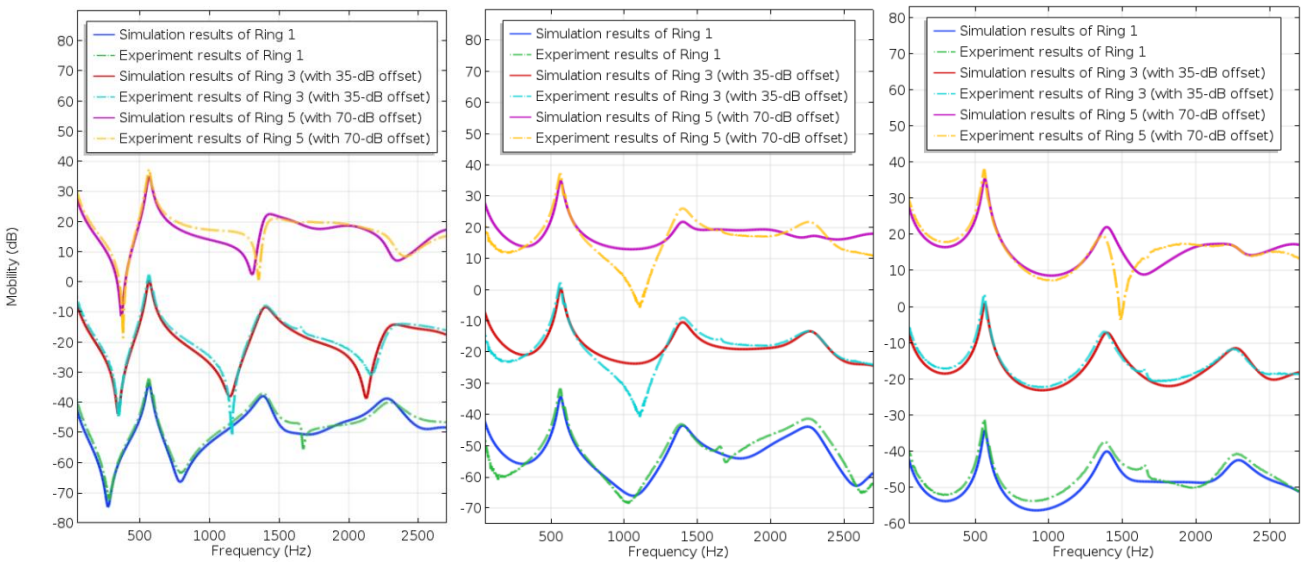

(a) (b) (c)

Figure 6: Comparisons of simulation and experiment results for the FRFs of five radially coupled rings in the radial direction at three different included angles, (a) 10°, (b) 90°, and (c) 180°, on the three rings (for clarity, each curve is offset from the one beneath by 35 dB).

Figure 7 compares the vibration responses of the two coupled rings and five coupled rings at two angles on each ring, and two obvious differences are observed. Firstly, different from two coupled rings, the responses of five coupled rings are much flatter, especially in the high frequency range. Only one peak of the first mode at 565 Hz is evident. This phenomenon should be caused by the increased accumulative energy transmission loss and damping effect when more rings are involved. Secondly, the peaks shift to higher frequency as the number of rings increases from two to five. A similar phenomenon occurs in the simulation of a single ring (presented in a forth-coming paper), in which the resonance frequencies decrease with the increase in the ring's radius. The average radius of five coupled rings is lower than that of two coupled rings. This shows, from another point of view, that the coupled rings vibrate like a single structure.

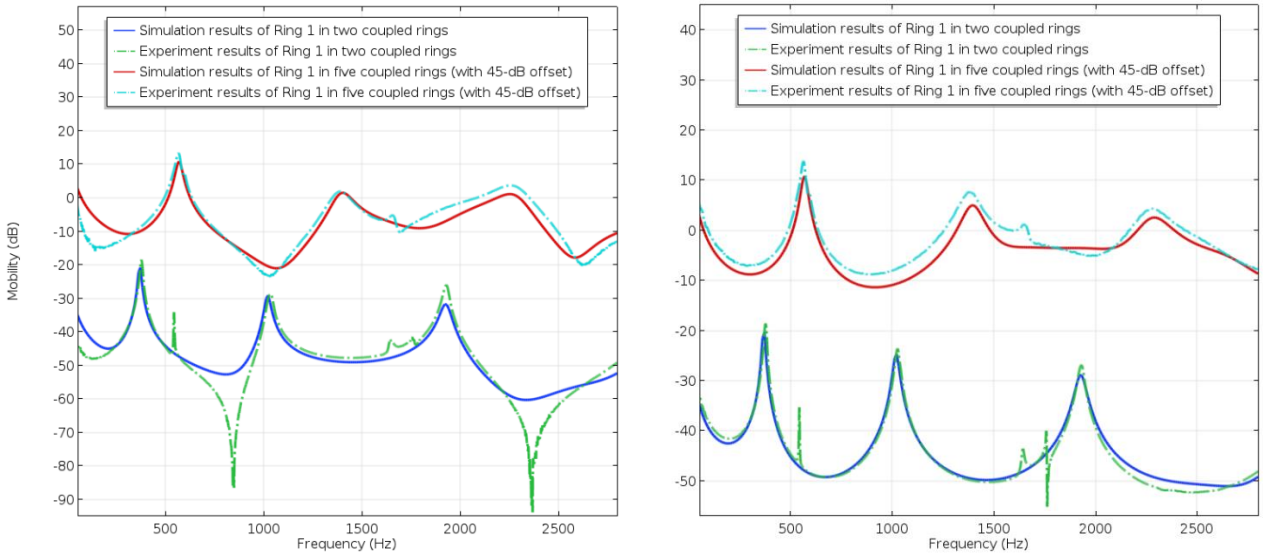

(a) (b)

Figure 7: Comparison of simulation and experiment results for the FRFs of two radially coupled rings and five radially coupled rings in the radial direction at two included angles, (a) 90° and (b) 180°, on Ring 1 (for clarity, each curve is offset from the one beneath by 45 dB).

5.3 Two-by-five coupled-ring stack

The vibration frequency responses at different included angles of excitation and measurement locations were shown previously, in the results for single-layer rings. Limited by this research paper, for the ring stack, only the vibration measured at the opposite locations of the hammer tapping point (*i.e.*, 180°) are given below. The FRFs of the two-by-five coupled-ring stack in the radial and axial directions are shown in Figure 8 and Figure 9.

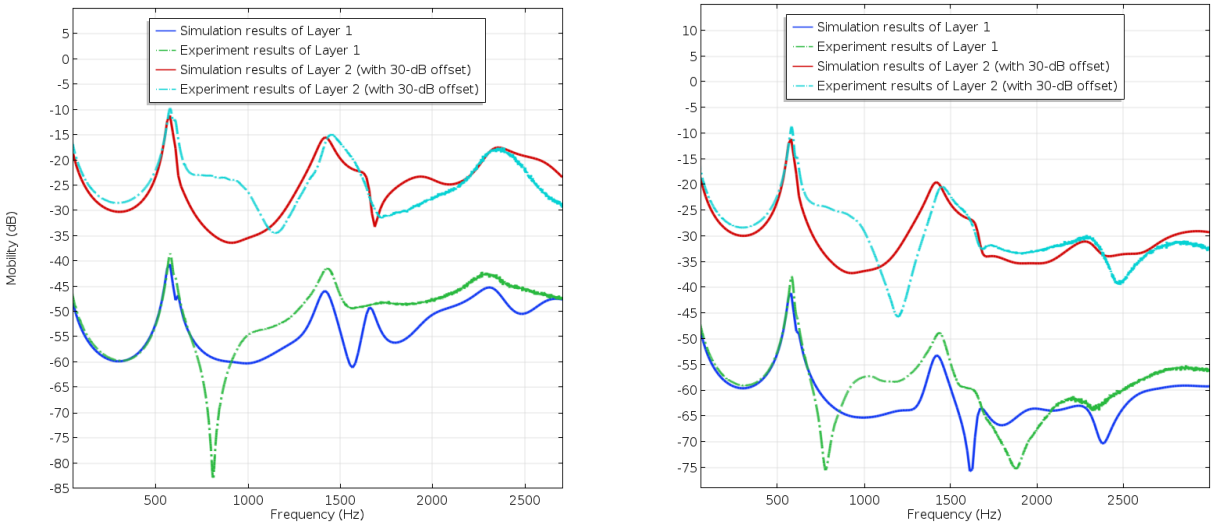

(a) (b)

Figure 8: Comparison of simulation and experiment results for the FRFs of the two-by-five coupled-ring stack in the radial direction on two rings, (a) Ring 1 and (b) Ring 5, on two layers (for clarity, each curve is offset from the one beneath by 30 dB).

It can be clearly observed from Figure 8 and Figure 9 that the FEM simulation results can reasonably predict the resonance frequencies and FRF trends of this stack. The simulated FEM curves appear flatter than the measured curves, in both two directions. The largest separation appears in the high-frequency range of the axial vibration response of the innermost ring (Ring 5). This suggests that the simulation settings have a greater impact on the rings as one moves inward and at higher frequencies.

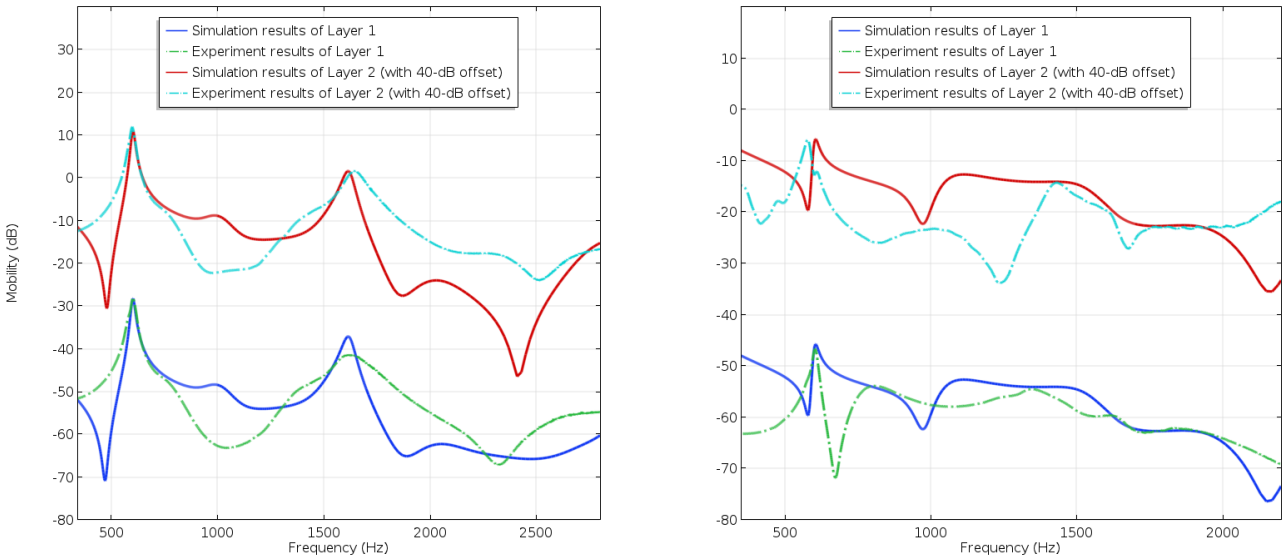

(a) (b)

Figure 9: Comparison of simulation and experiment results for the FRFs of the two-by-five coupled-ring stack in the axial direction on two rings, (a) Ring 1 and (b) Ring 5, on two layers (for clarity, each curve is offset from the one beneath by 40 dB).

For a comparison between the single-layer and multi-layer rings, the radial vibration of two rings in Layer 1 in the two-by-five coupled-ring stack and the corresponding rings in the five radially coupled rings are shown in Figure 10 and Figure 11, with the same included angles of excitation and measurement locations (180°).

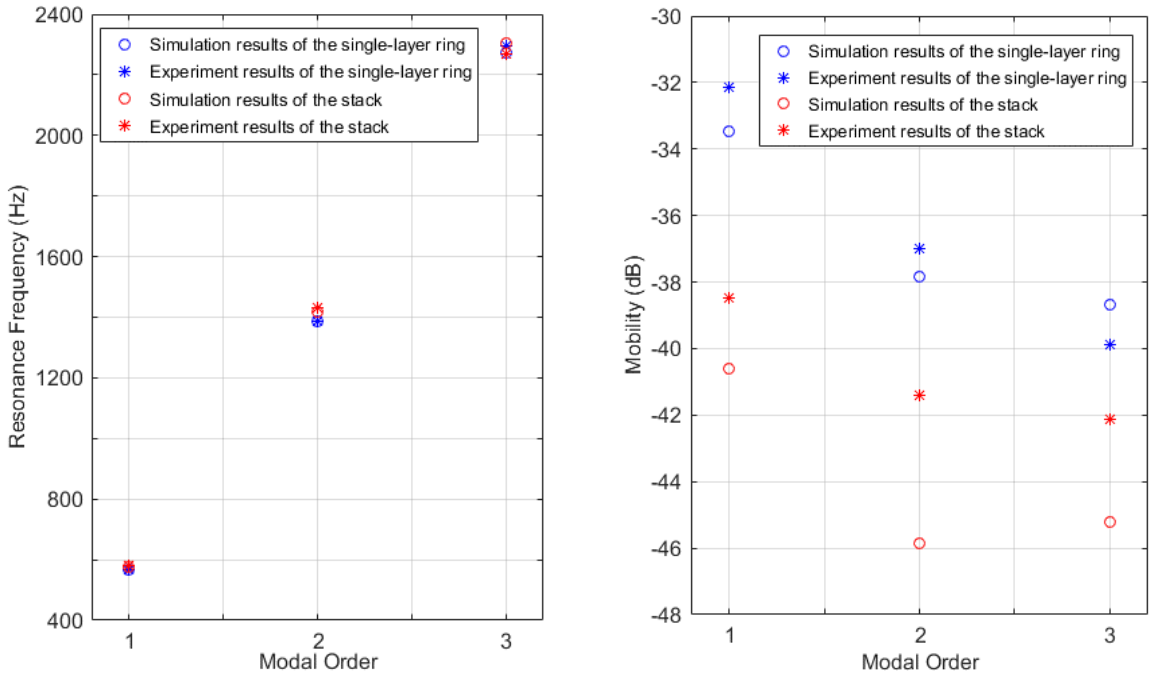

(a) (b)

Figure 10: Comparison of the simulation and experiment results for the first three (a) resonance frequencies and corresponding (b) mobility of five radially coupled rings and the Layer 1 of two-by-five coupled-ring stack in the radial direction on Ring 1, at an included angle of 180°.

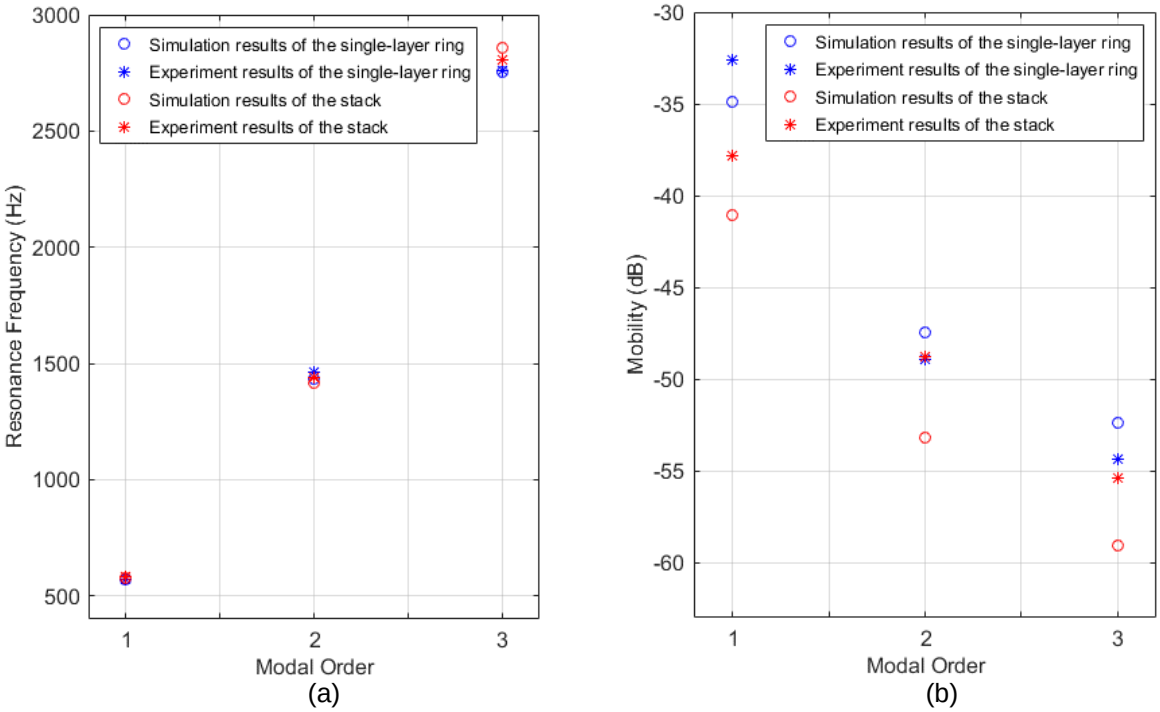

(a) (b)

Figure 11: Comparison of the simulation and experiment results for the first three (a) resonance frequencies and corresponding (b) mobility of five radially coupled rings and the Layer 1 of two-by-five coupled-ring stack in the radial direction on Ring 5, at an included angle of 180°.

The resonance frequencies in the multi-layer rings are slightly different from the single-layer, on both Ring 1 and Ring 5. The measured resonance frequencies on the second order of the single-layer and the stack on Ring 1, for example, are 1388 Hz and 1432 Hz, respectively. Mobility on the first three peaks of the FRFs of Ring 1 and Ring 5 in the stack are lower than in the single-layer rings, especially at lower frequencies and on the outer rings. These two differences may be caused by the friction between the rubber sticks and ring-layers.

6 CONCLUSION

A simplified but reasonable coupled-rings model was used to investigate the structural properties of disk-type windings in power transformers. The vibration behaviours of three different coupled-ring structures were detected through experiment and FEM simulation. The simulation results fit well with the experiments, indicating the correctness of the FEM parameters. However, the difference between the experiment and simulation FRF curves grew with the increasing number of coupled rings, which means the impact of errors is cumulative and becomes larger at higher frequencies. Meanwhile, coupled rings vibrate together like a single structure, and their resonance frequencies shift to a higher frequency range with an increasing number of rings. Finally, the resonance frequencies and corresponding mobility of FRFs for single-layer and multi-layer rings, with same number of radially coupled rings in one layer, have slight difference. The difference may be caused by the friction between the rubber sticks and ring-layers. These results and conclusions about coupled rings may help in understanding and investigating the structural characteristics of disk-type windings and they are thus meaningful for transformer noise control and condition monitoring.

ACKNOWLEDGEMENTS

This project was supported by the International Cooperation and Exchange Foundation for Doctoral Students of Zhejiang University and the China National Science Foundation (61603335, 11574269).

REFERENCES

Li, Lingzhi; Pan, Jie; Huang, Hai; Zheng, Jing; Hu, Yiwei; Zhang, Jiangong. 2017. 'Analytic Calculation and Analysis of the Magnetic Field for the Single-phase Two-limb Transformer'. *In Proceedings of the 12th IEEE Conference on Industrial Electronics and Applications (ICIEA)*, 2049–2054. Siem Reap, Cambodia.

Jin, Ming and Pan, Jie. 2015. 'Effects of Insulation Paper Ageing on the Vibration Characteristics of a Transformer Winding Disk'. *IEEE Transactions on Dielectrics and Electrical Insulation* 22 (6): 3560–3566.

Rausch, M.; Kaltenbacher, M.; Landes, H.; Lerch, R.; Anger, J.; Gerth, J.; Boss, P. 2002. 'Combination of Finite and Boundary Element Methods in Investigation and Prediction of Load-controlled Noise of Power Transformers'. *Journal of Sound and Vibration* 250 (2): 323–338.

Patel, Mukund. 1973. 'Dynamic Response of Power Transformers under Axial Short Circuit Forces Part I - Winding and Clamp as Individual Components'. *IEEE Transactions on Power Apparatus and Systems* 5: 1558–1566.

Booth, Campbell, and McDonald, Jim R. 1998. 'The Use of Artificial Neural Networks for Condition Monitoring of Electrical Power Transformers'. *Neurocomputing* 23 (1–3): 97–109.

Nguyen, T. 2007. 'Insulating the Windings', Master thesis, The University of Western Australia.

Jin, Ming. 2015. 'Vibration Characteristics of Power Transformers and Disk-type Windings', PhD thesis, The University of Western Australia.

Chidamparam, P., and Leissa, A. W. 1993. 'Vibration of planar curved beams, rings and arches', *Applied Mechanical Reviews*. 46 (9): 467–483.